Role of molecular phonons and interfacial-temperature discontinuities in water evaporation

Fei Duan and C. A. Ward*
Department of Mechanical and Industrial Engineering, University of Toronto, Thermodynamics and Kinetics Laboratory, 5 Kings's College Road, Toronto, Ontario, Canada M5S 3G8

V. K. Badam and F. Durst
Institute of Fluid Mechanics (LSTM), Friedrich-Alexander-Universität Erlangen-Nürnberg, Cauerstrasse 4, D-91058 Erlangen, Germany
(Received 23 May 2008; published 30 October 2008)

During steady-state water evaporation, when the vapor phase is heated electrically, the temperature on the vapor side of the interface has been reported to be as much as 27.83 °C greater than that on the liquid side. The reported interfacial temperatures were measured with thermocouple beads that were less than 50 μm in diameter and centered 35 μm from the interface in each phase. We examine the reliability of these measurements by using them with a theory of kinetics to predict the interfacial-liquid temperature. The predicted temperature discontinuities are found to be in agreement with those measured up to a temperature discontinuity of 15.69 °C, but larger discontinuities cannot be confirmed because of uncertainties in the vapor-phase pressure measurements. The theory of kinetics used in the analysis includes molecular phonons in the expression for the evaporation flux. We show it is essential to include these terms if the theory is to be used to predict the temperature discontinuities.

DOI: 10.1103/PhysRevE.78.041130 PACS number(s): 05.70.−a

I. INTRODUCTION

On a sunny day, when water evaporates from lakes, rivers, or oceans, the sun is the primary source of the energy transported to the water-air interface. It heats both the gas mixture at the interface and the liquid solution below the interface. In recent laboratory experiments in which the vapor was heated electrically, large interfacial temperature discontinuities were reported during steady-state water evaporation [1,2]. In each experiment, the interfacial-vapor temperature was reported to be greater than that of the liquid, reaching a maximum difference of 27.83 °C. Earlier measurements of the interfacial fluid temperatures during evaporation, without electrical heating, reported temperature discontinuities for water and for other liquids, but the maximum temperature discontinuity was found for water and was only 7.8 °C [3–10].

Clearly, heating the vapor during evaporation is indicated to strongly influence the conditions at the interface, but the temperature discontinuities produced are so large that one would like to be assured they are correct, especially since all of the measurements that have indicated interfacial-temperature discontinuities during evaporation have been made with microthermocouples (bead diameters <50 μm). Interferometer measurements of the temperature profile in the liquid phase during evaporation have been attempted, but this technique is difficult to apply near the interface. For example, Barnes and Feher [11] used interferometry to measure the temperature during water evaporation, but their first data point in the liquid was 125 μm below the interface and their second was 625 μm below. When microthermocouples are used, the center of the thermocouple bead in the liquid or vapor phase is approximately 35 μm away from the interface, and the surface of the bead is 10 μm away. Measurements made with microthermocouples have indicated the presence of a "uniform-temperature layer" when thermocapillary convection is present that can extend to a depth of 100 μm [5–10], but the interferometry method did not detect this layer. Its absence led several investigators to conclude there was no evidence of thermocapillary (or Marangoni) convection during water evaporation [12]. However, the presence of thermocapillary convection during water evaporation was subsequently demonstrated with a flow probe [7]. Also, an energy balance cannot be shown to exist at the interface during either H_2O or D_2O evaporation, unless energy transport by thermocapillary convection is taken into account [8–10], and later, Xu and Luo [13] also reported evidence of thermocapillary (or Marangoni) convection during water evaporation. Thus, although not detected by interferometry, there is now strong evidence of Marangoni convection in water.

Another method by which the existence of interfacial-temperature discontinuities can be examined is to consider their consistency with theory. Molecular-dynamic simulations were used by Hołyst and Litniewski [14] to model the evaporation of a Lennard-Jones fluid. They concluded the interfacial-vapor temperature would be greater than that of the liquid if the liquid density were more than ten times that of the vapor. When the vapor is heated, this density ratio would be increased, but in the experiments we consider, it is of order 10^3, without heating. Thus the existence of interfacial-temperature discontinuities with the temperature greater in the vapor than in the liquid during evaporation appears consistent with molecular-dynamic simulations, but the question remains: are the measured temperature discontinuities quantitatively correct?

Statistical rate theory (SRT) [15,16] can be applied to investigate this question. It gives the expression for the evaporation flux in terms of the entropy change resulting from one molecule going from the liquid to the vapor [3,17]. This entropy change is the sum of two terms. One results

*ward@mie.utoronto.ca

from continuum effects, is positive, and acts as the driving-force for evaporation. It only depends on the interfacial-*liquid* temperature. The other entropy-change term is negative, depends on the phonon structure of the water molecule, and depends on the interfacial-temperature discontinuity. We find that neither of these terms is negligible, and in order to predict the temperature discontinuity, the phonon term must be included.

The SRT approach was examined recently [18] when interfacial temperature discontinuities of up to 7.8 °C were present. Its expression for the evaporation flux contains the equilibrium-saturation-vapor pressure, $P_s(T)$, as a parameter, and the SRT expression for the evaporation flux can be used to determine the value of $P_s(T)$ from measurements of the evaporation flux and the interfacial temperatures and pressures. Measurements in 50 different evaporation or condensation experiments for temperatures from the triple point down to −19.26 °C were used. In this temperature range, $P_s(T)$ was not well-established, since the liquid phase is metastable and susceptible to ice formation. From the analytical expression for $P_s(T)$ obtained from SRT, the latent heat of evaporation, L_{lv}, and the constant pressure specific heat of the liquid, c_p^L, were predicted, and compared with independent measurements. The predicted values of both L_{lv} and c_p^L were in agreement with the measurements over a range of temperatures.

Since SRT is indicated to be capable of reliably predicting the evaporation flux [18] and $P_s(T)$ for water below the triple point is now available, we report the application of SRT and the expression for $P_s(T)$ to predict the temperature discontinuities in three different circumstances: steady-state water evaporation from: (1) a polymethylmethacrylate (PMMA) funnel with a circular mouth in which the maximum measured temperature discontinuity reached 5.69 °C; (2) a stainless-steel funnel with a rectangular mouth opening that gave temperature discontinuities up to 2.46 °C; and (3) two sets of water evaporation experiments conducted with a polyvinylchloride (PVC) funnel that had a rectangular mouth opening. In one set of these experiments, an electrical heater in the vapor phase had temperatures up to 80 °C and in the other, a vapor phase heater had values up to 200 °C.

The first two of these circumstances provides new data, and the SRT expression for the evaporation flux is different in each case because the liquid-vapor interface was spherical in one case and cylindrical in the other. In neither of these cases was the vapor heated. The data in the third case is that of [1,2] in which the vapor phase was electrically heated, and the reported discontinuities were as large as 27.83 °C. The measured-temperature discontinuities up to 15.69 °C are found to be consistent with SRT, but no conclusion can be drawn regarding the measurements of the larger discontinuities because of uncertainties in the vapor-phase pressure measurements.

II. EXPERIMENTAL METHODS

The procedures and apparatuses used in these experiments have been previously described [1,2,5,6,9]. Briefly, in preparation for an experiment, purified water (resistivity $\geqslant$18 MΩ cm) was placed in a (borosilicate) glass cylinder where the vapor phase was connected through a valving system to a vacuum pump that allowed the liquid to be degassed, and then, without exposure to air, to be transferred into a syringe and pumped into the bottom of one of the funnels described above. The temperature of the water entering a funnel was maintained slightly less than 4 °C. The water was pumped further until it reached the funnel mouth. If the funnel had a rectangular mouth opening, the liquid-vapor interface was cylindrically shaped, and if the funnel mouth were circular, the liquid-vapor interface was spherical. The water at the funnel mouth was exposed to the pressure of the evaporation chamber that was controlled by a vacuum system. The evaporation at the interface cooled the liquid there below that at the funnel throat, and since water has its maximum density at 4 °C the lighter liquid was above the heavier, eliminating the possibility of buoyancy-driven convection in each of the experiments. The pressure in the evaporation chamber and the pumping rate were adjusted so the liquid-vapor interface was unmoving while the water evaporated steadily. The interface had a maximum height above the funnel mouth of 1 mm. With the liquid evaporating steadily, the temperature in the liquid and vapor phases was measured with a thermocouple constructed with 25-μm-diameter wires that were formed into a U shape, had a bead diameter $\leqslant$50 μm [6], and was mounted on a positioning micrometer.

A. Position of temperature measurements relative to the interface

If the vapor-phase molecules are approximated as hard spheres, the value of their diameter, d_m, may be estimated from the dynamic viscosity, η_{vap} [19]:

$$d_m = \left[\frac{1}{3\pi\eta_{vap}} \sqrt{\frac{3m_w k_b T}{2}} \right]^{1/2}, \tag{1}$$

where k_b is the Boltzmann constant and m_w is the molecular mass. The mean-free path in the vapor, P_{mf}, is approximately given by

$$P_{mf} = \frac{k_b T}{\sqrt{2}\pi d_m^2}. \tag{2}$$

The calculated value of the mean-free path in the vapor phase of each experiment is listed in Tables I–IV. In each case, the center of the thermocouple bead in the vapor was less than 6 P_{mf} from the interface, and in some of our experiments, it was less than one mean-free path. Thus, we take the temperature measured closest to the interface in the vapor as approximately equal to the interfacial-vapor temperature.

In the liquid phase, experiments previously performed with the stainless-steel funnel indicated the presence of thermocapillary convection [7,9]. As a result of the fluid mixing produced by this convection, immediately below the interface, on the centerline, there was a uniform-temperature layer that was at least 50 μm deep. The position of the center of the thermocouple bead when the temperature closest to the interface was measured was less than 35 μm below the in-

TABLE I. Thermal conditions in liquid and vapor phases on the funnel centerline measured during steady-state water evaporation from a PMMA funnel. For those experiments labelled NA there was no heating element.

Expt.:	Heat element temp. (°C)	Measured vapor-phase (Press./Pa)	Predicted vapor-phase (Press./Pa)	Local evap. flux (mg/m^2 s)	Interface vapor temp. (°C)	Interface liquid temp. (°C)	Interface curv. C_0 (m^{-1})	Mean-free path (μm)
EA1	NA	176.0	173.9	865.0	−10.46	−16.15	126.90	30.9
EA2	NA	196.0	195.1	848.9	−9.48	−14.77	140.49	27.8
EA3	NA	595.9	594.4	456.3	1.77	−0.37	184.30	9.6
EA4	NA	611.9	612.4	398.4	1.98	0.04	150.94	9.3
EA5	NA	590.6	592.3	298.2	1.48	−0.42	147.06	9.7
EA6	NA	587.9	587.9	134.7	1.31	−0.52	149.66	9.7
EA7	NA	341.3	342.4	700.4	−4.17	−7.72	154.75	16.3
EA8	NA	485.3	486.1	568.3	−0.41	−3.10	153.52	11.7

terface, and thus was within the uniform-temperature layer. Hence, in each of the experiments with the stainless-steel funnel, the temperature measured in the liquid phase closest to the interface may be taken as the interfacial liquid temperature.

In the experiments performed with the PMMA and PVC funnels, no uniform temperature layer was reported [18,1,2], but we assume that the temperature measured closest to the interface in the liquid-phase for the experiments described in Tables I, III, and IV were equal to the interfacial-liquid temperatures.

B. Determination of the local evaporation flux

Symmetry considerations indicate the thermocapillary convection would vanish on the centerline of both a cylindrical liquid-vapor interface and a spherical liquid-vapor interface. If the temperature is measured in the liquid and vapor phases as a function of height at a position where the thermocapillary convection may be neglected, the local evaporation flux, j_{ev}, may be expressed in terms of the measured temperature gradients, $\nabla T^L, \nabla T^V$, the thermal conductivities, κ^L, κ^V, and the enthalpies h^V, h^L in the liquid and vapor phases evaluated at the interface:

$$j_{ev} = \frac{(-\kappa^L \nabla T^L \cdot \iota_r + \kappa^V \nabla T^V \cdot \iota_r)}{h^V(T_I^V) - h^L(T_I^L)}, \tag{3}$$

where ι_r is the unit vector normal to the liquid-vapor interface. The enthalpies at the triple point, T_{tp}, are well-documented. If the temperatures at the interface in the liquid and vapor phases are denoted T_I^L and T_I^V, the enthalpy difference may be written [7]

$$h^V(T_I^V) - h^L(T_I^L) = h_{fg}(T_{tp}) + c_p^V(T_I^V - T_{tp}) - c_p^L(T_I^L - T_{tp}), \tag{4}$$

where c_p^L and c_p^V denote the constant pressure specific heat of the liquid and vapor phases evaluated at T_{tp}.

C. Experiments without electrical heating of the vapor phase

The conditions at the interface during the experiments conducted with a PMMA funnel are summarized in Table I. The maximum interfacial temperature discontinuity observed was in experiment EA1: the interfacial-vapor temperature was 5.69 °C greater than that of the liquid. The temperature measured as a function of depth in this experiment is shown in Fig. 1. The maximum evaporation flux with this funnel was also observed with this experiment.

TABLE II. Thermal conditions in liquid and vapor phases during steady-state water evaporation from a stainless-steel funnel. For those experiments labelled NA there was no heating element.

Expt.:	Heat element temp. (°C)	measured vapor-phase (Press./Pa)	Predicted vapor-phase (Press./Pa)	Local evap. flux (mg/m^2 s)	Interface-vapor temp. (°C)	Interface liquid temp. (°C)	Interface-curv. C (m^{-1})	Mean-free path (μm)
EO1	NA	799.9	795.7	141.1	4.63	3.69	123.24	7.2
EO2	NA	719.9	724.0	173.1	3.50	2.36	117.65	8.0
EO3	NA	589.3	592.1	372.7	0.70	−0.42	126.84	9.6
EO4	NA	461.3	462.2	599.6	−2.19	−3.77	125.83	12.2
EO5	NA	346.6	343.2	894.9	−5.95	−7.68	117.65	16.0
EO6	NA	274.6	271.1	1150.0	−8.88	−10.68	119.72	19.9
EO7	NA	220.0	219.2	1269.6	−10.84	−13.32	122.79	24.7

TABLE III. Thermal conditions in liquid and vapor phases on the central plane of a PVC funnel (see Fig. 2) measured during steady-state water evaporation [1]. In some of the experiments, an electrical heater was activated and its temperature set at one of the indicated temperatures. In other experiments, the heater was turned-off, denoted NA in the table.

Expt.:	Heat element temp. (°C)	Measured vapor-phase (Press./Pa)	Predicted vapor-phase (Press./Pa)	Local evap. flux ($mg/m^2\,s$)	Interface vapor temp. (°C)	Interface liquid temp. (°C)	Interface curv. C (m^{-1})	Mean-free path (μm)
Eh1	NA	561.0	563.4	268.6	0.73	−1.10	117.65	10.1
Eh2	NA	490.0	491.1	278.5	−0.93	−2.96	115.29	11.5
Eh3	NA	389.1	390.1	316.0	−3.76	−6.02	117.65	14.3
Eh4	NA	336.5	337.6	335.1	−5.29	−7.90	115.29	16.5
Eh5	NA	292.4	295.3	348.4	−6.83	−9.61	115.29	18.8
Eh6	NA	245.3	250.8	342.1	−8.42	−11.67	114.12	22.3
Eh7	30	736.0	738.8	343.9	6.64	2.65	117.65	7.9
Eh8	30	569.5	571.1	367.9	2.93	−0.91	117.65	10.1
Eh9	30	483.3	482.9	378.0	1.04	−3.18	118.82	11.8
Eh10	30	391.2	389.8	417.9	−1.26	−6.02	117.65	14.4
Eh11	30	295.2	297.4	435.3	−4.01	−9.51	118.82	18.9
Eh12	30	240.3	247.0	505.5	−6.09	−11.85	114.12	23.0
Eh13	40	736.0	738.5	411.8	7.97	2.65	122.35	8.0
Eh14	40	567.0	568.3	426.5	4.82	−0.97	117.65	10.2
Eh15	40	485.0	484.7	463.7	3.02	−3.12	110.59	11.8
Eh16	40	392.3	391.7	465.1	0.57	−5.95	105.88	14.5
Eh17	40	288.5	290.5	526.5	−2.22	−9.80	117.65	19.5
Eh18	40	236.6	240.2	539.8	−4.00	−12.18	118.82	23.6
Eh19	50	847.9	850.7	514.2	10.91	4.66	118.82	7.0
Eh20	50	743.0	745.6	500.4	9.50	2.79	117.65	7.9
Eh21	50	572.4	570.0	500.7	6.37	−0.92	122.35	10.2
Eh22	50	391.4	388.9	549.9	2.77	−6.03	117.65	14.6
Eh23	50	288.5	289.7	572.7	−0.12	−9.82	117.65	19.6
Eh24	50	236.0	239.4	595.9	−1.97	−12.21	117.65	23.8
Eh25	60	866.0	872.9	675.3	12.90	5.04	117.65	6.9
Eh26	60	743.9	745.6	627.4	11.07	2.80	118.82	8.0
Eh27	60	569.2	569.6	622.2	7.96	−0.92	117.65	10.3
Eh28	60	386.3	390.4	658.4	3.83	−5.97	112.94	14.9
Eh29	60	291.7	299.0	708.9	1.33	−9.41	117.65	19.5
Eh30	60	235.5	242.4	719.3	−0.54	−12.04	114.12	24.0
Eh31	70	966.8	973.7	766.4	10.72	6.62	104.71	6.1
Eh32	70	850.5	855.2	726.7	13.37	4.75	111.76	7.1
Eh33	70	747.0	748.3	723.6	12.38	2.86	112.94	8.0
Eh34	70	573.1	571.2	682.4	9.60	−0.87	117.65	10.3
Eh35	70	389.2	390.9	711.0	5.56	−5.94	107.06	14.9
Eh36	70	290.7	294.6	746.5	3.23	−9.58	118.82	19.8
Eh37	70	215.6	224.0	759.7	1.63	−12.99	118.82	26.5
Eh38	80	1076.8	1072.9	779.7	17.82	8.11	114.12	5.7
Eh39	80	946.3	959.5	847.8	15.95	6.43	115.29	6.4
Eh40	80	855.1	852.2	794.4	14.90	4.71	123.53	7.1
Eh41	80	744.5	751.0	816.4	13.68	2.92	117.65	8.1
Eh42	80	569.2	575.0	779.2	10.84	−0.77	121.18	10.4
Eh43	80	388.7	389.7	789.0	7.77	−5.96	115.29	15.1
Eh44	80	288.1	290.1	751.1	4.69	−9.76	116.47	20.1
Eh45	80	213.0	216.1	764.3	2.27	−13.42	112.94	26.8

TABLE IV. Thermal conditions in liquid and vapor phases during steady-state water evaporation from the PVC channel (see Fig.2) when the heating element was set a temperatures between 100 and 200 °C [2].

Expt.:	Heat element temp. (°C)	Measured vapor-phase (Press./Pa)	Predicted vapor-phase (Press./Pa)	Local evap. flux (mg/m^2 s)	Interface vapor temp. (°C)	Interface liquid temp. (°C)	Interface curv. C (m^{-1})	Mean-free path (μm)
Eh46	100	514.0	760.3	531.0	13.76	3.09	122.79	11.7
Eh47	130	309.0	893.9	772.0	21.10	5.45	117.65	20.1
Eh48	150	306.0	676.3	894.0	20.30	1.54	126.84	20.3
Eh49	175	308.7	394.0	2271.0	20.84	−5.62	125.83	20.1
Eh50	200	306.5	510.9	1918.0	25.68	−2.14	117.65	20.7

The interfacial conditions during the experiments with the stainless-steel funnel are summarized in Table II. The largest interfacial temperature discontinuity, 2.48 °C, was observed in experiment EO7. The temperature as a function of height measured during this experiment is shown in Fig. 1. The evaporation flux was also a maximum in this experiment.

D. Experiments in which the vapor was electrically heated

A schematic of the test section used in these experiments is shown in Fig. 2, and the experimental conditions are listed in Tables III and IV. The experiments are divided into two types, depending on the maximum temperature of the heating element.

1. Heating-element temperatures up to 80 °C

Experiments were conducted both with the constantan-heating element turned-off (see Fig. 2) and with it set at one of the temperatures indicated in Table III. The heating element was placed approximately 4 mm above the liquid-vapor interface. The largest interfacial-temperature discontinuity observed was 15.69 °C. Both the vapor-phase pressure and the temperature of the heating element are seen to play a role in determining the temperature discontinuity. In Fig. 1 the temperature measured as a function of depth in Eh45 is shown.

2. Heating-element temperatures from 100 to 200 °C

If the interfacial temperature discontinuities listed in Tables I and II are compared with those listed in Table III, it is clear that electrically heating the vapor produced larger temperature discontinuities. In an effort to obtain even higher interfacial temperature discontinuities, the constantan-heating element used in the apparatus shown schematically in Fig. 2 was replaced by a platinum-mica element that could be set at temperatures up to 200 °C. This heating element was placed approximately 3 mm above the liquid vapor interface. The conditions in the evaporation chamber during this series of five experiments are listed in Table IV. The measured interfacial temperature discontinuity reached 27.82 °C in experiment Eh50.

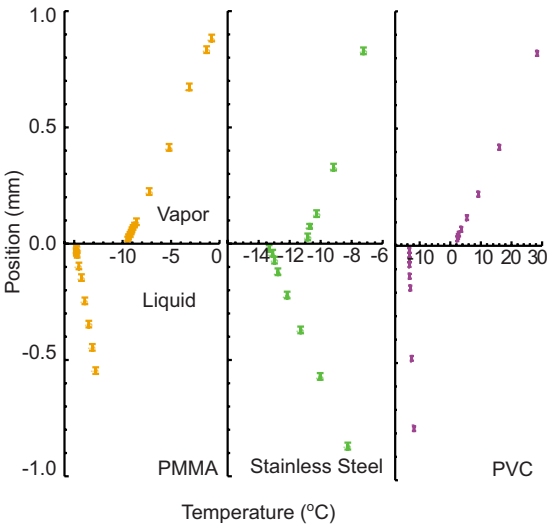

FIG. 1. (Color online) Temperatures measured as a function of depth in the liquid and vapor phases during steady-state evaporation when the liquid was held in a PMMA funnel (EA1, I), in a stainless-steel (EO7, Table II) or in a PVC funnel (EH45, Table III). Note the different magnitudes of the interfacial temperature discontinuities.

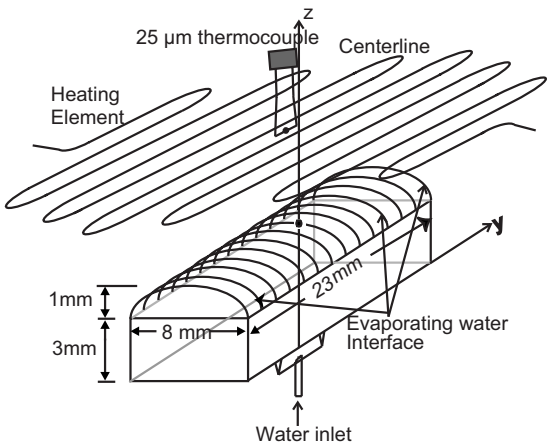

FIG. 2. Schematic of the polyvinylchloride funnel with a rectangular mouth opening [1,2]. This funnel was enclosed in a chamber that allowed the thermocouple to be monitored from outside. The constantan-heating-element temperature could be set as high as 80 °C during steady-state water evaporation. See Table III. In a second set of experiments, a platinum-mica heating element that could be set up to a temperature of 200 °C replaced the constantan-heating-element. See Table IV.

III. STATISTICAL RATE THEORY EXPRESSION FOR EVAPORATION FLUX

The SRT expression for the net evaporation flux, j_{ev}, has been obtained from the transition probability concept of quantum mechanics, the Boltzmann definition of entropy, and a hypothesis that supposes the exchange rate between quantum mechanical states of an isolated system is the same for any pair of states [4,5,9,10,17,18]. Local equilibrium is assumed to exist at the interface within the liquid and within the vapor, but disequilibrium to exist across the interface. Then if K_e is defined as

$$K_e \equiv \frac{P_s(T_I^L)\exp\{(v_f/v_g)[P_I^L/P_s(T_I^L)-1]\}}{\sqrt{2\pi m_w k_b T_I^L}}, \tag{5}$$

where and v_f and v_g denote the specific volume of the saturated liquid and vapor phases, respectively, and Δs_{LV} denotes the change in entropy that results from one molecule going from the liquid to the vapor phase, the SRT expression for the net flux of molecules from the liquid to the vapor phase at one instant is given by

$$j_{ev} = 2K_e \sinh\left(\frac{\Delta s_{LV}}{k_b}\right). \tag{6}$$

If the chemical potentials of the molecules in the liquid and the vapor phases at the interface are denoted as μ_I^L, μ_I^V, the interfacial temperatures as T_I^L, T_I^V, and the interfacial enthalpy of the vapor as h_I^V, then [17]

$$\Delta s_{LV} = \left(\frac{\mu_I^L}{T_I^L} - \frac{\mu_I^V}{T_I^V}\right) + h_I^V\left(\frac{1}{T_I^V} - \frac{1}{T_I^L}\right). \tag{7}$$

Note that the SRT expression for j_{ev} allows both the chemical potential and the temperature to be discontinuous across the interface.

The SRT expression for the evaporation flux may be written in terms of measurable quantities by expressing the chemical potential of the liquid-phase molecules in terms of that of the vapor-phase molecules and approximating the vapor as an ideal gas [4]. If the saturation-vapor pressure is denoted $P_s(T)$, then by definition

$$\mu^L[T^L, P_s(T^L)] = \mu^V[T^L, P_s(T^L)]. \tag{8}$$

Provided the liquid-phase pressure is not too large,

$$|\kappa_T(P^L - P_s)| \ll 1, \tag{9}$$

where κ_T is the isothermal compressibility, the chemical potential of the liquid phase may be expressed as

$$\mu^L(T^L, P^L) = \mu^V[T^L, P_s(T^L)] + v_f(T^L)[P^L - P_s(T^L)], \tag{10}$$

If the surface tension is denoted γ^{LV} and C_1 and C_2 are the interface curvatures, the Laplace equation relates the pressure in the liquid to that in the vapor,

$$P_I^L = P_I^V + \gamma^{LV}(C_1 + C_2). \tag{11}$$

When the vapor phase is approximated as an ideal gas, the chemical potential of the vapor-phase molecules may be written as

$$\mu^V(T^V, P^V) = \mu^V[T^V, P_s(T^V)] + k_b T^V \ln\left[\frac{P^V}{P_s(T^V)}\right]. \tag{12}$$

Equations (10)–(12) may now be substituted into Eq. (7); however, the expression would contain $\mu^V[T^L, P_s(T^L)]$, $\mu^V[T^V P_s(T^V)]$, and $h_I^V(T_I^V)$. Statistical thermodynamics may be applied to determine the expressions for these functions in terms of T_I^V and T_I^L. If the fundamental vibration frequencies of the triatomic water molecule are denoted ω_l ($l=1$, 2, or 3), the expression for Δs_{LV} may be written as [4,5,17]

$$\begin{aligned}\frac{\Delta s_{LV}}{k_b} &= 4\left(1 - \frac{T_I^V}{T_I^L}\right) + \left(\frac{1}{k_b T_I^V} - \frac{1}{k_b T_I^L}\right)\sum_{l=1}^{3}[\hbar\omega_l \eta(\omega_l, T^V)] \\ &+ \frac{v_f}{k_b T_I^L}[P_I^V + \gamma^{LV}(C_1 + C_2) - P_s(T_I^L)] \\ &+ \ln\left[\left(\frac{T_I^V}{T_I^L}\right)^4\left(\frac{P_s(T_I^L)}{P_I^V}\right)\left(\frac{q_{vib}(T_I^V)}{q_{vib}(T_I^L)}\right)\right],\end{aligned} \tag{13}$$

where the average number of each type of phonon per molecule, $\eta(\omega_l, T)$, is given by

$$\eta(\omega_l, T^V) = \frac{\left[\exp\left(\frac{\hbar\omega_l}{k_b T_I^V}\right) + 1\right]}{\left[2\exp\left(\frac{\hbar\omega_l}{k_b T_I^V}\right) - 2\right]}, \tag{14}$$

and the vibration partition function is given by

$$q_{vib}(T) \equiv \prod_{l=1}^{3} \frac{\exp(-\hbar\omega_l/2k_b T)}{1 - \exp(-\hbar\omega_l/k_b T)}. \tag{15}$$

The vibration frequencies of the covalent bonds of the water molecule involve combinations of symmetric stretch (3651 cm^{-1}), asymmetric stretch (3756 cm^{-1}), and bending (1590 cm^{-1}) [20].

The expression for $P_s(T)$ at temperatures below the triple point was established in Ref. [18]:

$$\begin{aligned}P_s = 611.2\exp[&1045.851\,157\,7 - 21\,394.666\,262\,9/T \\ &+ 1.096\,904\,4T - 1.300\,374\,1\times10^{-3}T^2 + 7.747\,298\,4 \\ &\times 10^{-7}T^3 - 2.164\,900\,5\times10^{-12}T^4 \\ &- 211.389\,655\,9\ln T].\end{aligned} \tag{16}$$

We take the surface tension to be given by [21]

$$\begin{aligned}\gamma^{LV} = 10^{-3}[&75.478\,70 - 0.138\,48(T - 273.15) - 3.363\,92 \\ &\times 10^{-4}(T - 273.15)^2 + 4.753\,62\times10^{-7}(T - 273.15)^3 \\ &+ 2.644\,79\times10^{-10}(T - 273.15)^4],\end{aligned} \tag{17}$$

and the specific volume of the saturated liquid to be given by [22]

$$\begin{aligned}v_f = 10^{-3}(&334.601\,163 - 6.962\,367T + 6.067\,943\times10^{-2}T^2 \\ &- 2.825\,583\times10^{-4}T^3 + 7.411\,762\times10^{-7}T^4 \\ &- 1.038\,083\times10^{-9}T^5 + 6.063\,848\,4\times10^{-13}T^6).\end{aligned} \tag{18}$$

When Eqs. (5), (11), (13), (17), and (18) are combined with

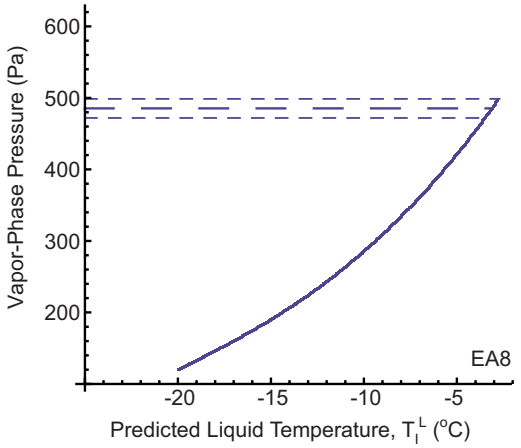

FIG. 3. (Color online) The iteration procedure used to calculate the temperature discontinuity for experiment EA8, Table I is illustrated.

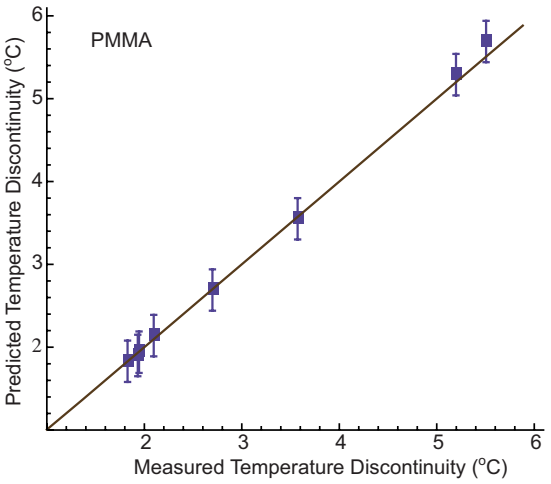

FIG. 4. (Color online) The calculated value of the interfacial temperature discontinuity compared with that measured when water evaporated at the circular mouth of a PMMA funnel. The error bars reflect the uncertainty in the vapor-phase pressure measurements.

Eq. (6), one obtains an expression for the evaporation flux that is in terms of the instantaneous interfacial properties T_I^L, T_I^V, P_I^V, C_1, and C_2.

Prediction of the temperature discontinuity

In each experiment described in Tables I–IV, the measured values of j_{ev}, T_I^V, T_I^L, P_I^V and the curvatures C_1 and C_2 are listed. Thus the interfacial temperature discontinuity ($\equiv T_I^V - T_I^L$) can be directly determined from the measurements. We show that if j_{ev}, T_I^V, P_I^V, C_1, and C_2 are known, then SRT can be used to predict T_I^L, from which the interfacial temperature discontinuity can be calculated. The interfacial temperature discontinuity determined from this procedure may then be compared with that measured to assess the consistency of the measured temperature discontinuity with the SRT predictions.

The iterative procedure begins by assuming a value of T_I^L, then from given values of j_{ev}, T_I^V, C_1, and C_2, Eqs. (5), (11), (16), and (6) are used to calculate a value of P_I^V corresponding to the assumed value of T_I^L. This calculated value of P_I^V is then compared with the measured value of P_I^V. If they differ by more than ± 13 Pa, another value of T_I^L is assumed and the procedure repeated until a value of P_I^V of sufficient accuracy is obtained.

The calculation procedure is illustrated in Fig. 3 for experiment EA8 of Table I. For the experiments described in this table, the funnel was constructed of PMMA and the funnel mouth was circular, resulting in a spherical liquid-vapor interface. Thus C_1 was equal to C_2, denoted C_0 in Table I. For experiment EA8, the value of the vapor-phase pressure that was measured is indicated by the long-dashed line in Fig. 3. The possible measurement error in the pressure is illustrated by the two short-dashed lines. In the illustration, the first value chosen for T_I^L was 17 °C less than the measured interfacial-vapor-phase temperature. The calculated value of the vapor-phase pressure corresponding to this value of T_I^L was approximately 50 Pa (see Fig. 3), whereas the measured pressure was almost 500 Pa. A series of T_I^L values were assumed to obtain the solid curve shown in Fig. 3. The predicted value of the temperature discontinuity is reached when the calculated value of the vapor-phase pressure is equal to the measured value $\pm$ the pressure-measurement error. In this experiment, the calculated value of T_I^L was 3 °C.

The calculated values of the interfacial-temperature discontinuity obtained for the other experiments described in Table I are shown in Fig. 4, where they may be compared with the measured values of the temperature discontinuities in each of the experiments. The error bars on each prediction reflects the accuracy with which the vapor-phase pressure could be measured. For the experiments with spherical liquid-vapor interfaces, there were no measurable differences between the predicted and measured temperature discontinuities.

For the experiments described in Table II, the funnel was constructed of stainless steel and had a rectangular mouth opening. The curvature of the resulting cylindrical liquid-vapor interface is denoted as C in Table II. Changing these parameters resulted in changes in the heat flux to the interface, as indicated in Fig. 1. Note that the SRT expression for the evaporation flux depends on the curvature of the interface [see Eq. (13)]. The procedure outlined earlier was used to calculate the temperature discontinuity in this case as well. The results obtained are shown in Fig. 5 where they may be compared with the measurements. As found for the measurements made at the spherical liquid-vapor interface, when the liquid-vapor interface was cylindrical, there were no measurable differences between the predicted and the measured temperature discontinuities.

In the experiments described in Table III an important parameter was changed: the vapor-phase temperature at the interface was altered by electrically heating the vapor phase at a position above the interface. Heating the vapor phase gave rise to the large interfacial-temperature discontinuities indicated in Table III. Statistical rate theory indicates that the evaporation flux depends on the local properties at the interface; thus we suppose the interfacial-vapor temperature mea-

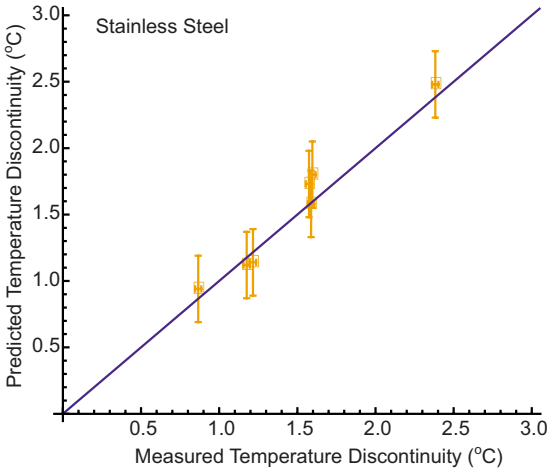

FIG. 5. (Color online) The calculated value of the interfacial temperature discontinuity compared with that measured when water evaporated at the rectangular mouth of a stainless-steel funnel. The error bars reflect the uncertainty in the vapor-phase pressure measurements.

sured with a thermocouple reflects the actual temperature there.

We examine the hypothesis by using the measured interfacial-vapor temperature with SRT to predict the interfacial-liquid temperature using the method described earlier. Following that procedure, but using the data listed in Table III, one finds the results shown in Fig. 6. As with the results shown in Figs. 4 and 5, there is no disagreement between the predictions and the measurements. Nor is there any trend indicating disagreement developing as the measured temperature discontinuity became larger. Thus the SRT calculations are consistent with the temperature discontinui-

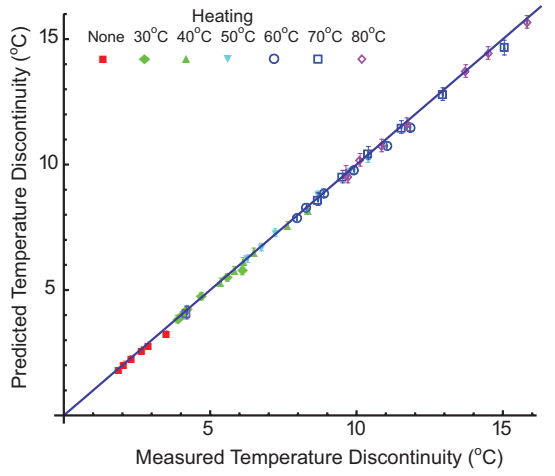

FIG. 6. (Color) The calculated value of the interfacial temperature discontinuity compared with that measured when water evaporated at the rectangular mouth of a PVC funnel. In some of the experiments the vapor phase was heated up to a maximum of 80 °C (Table III) at a position approximately 4 mm above the liquid-vapor interface. The error bars reflect the uncertainty in the vapor-phase pressure measurements.

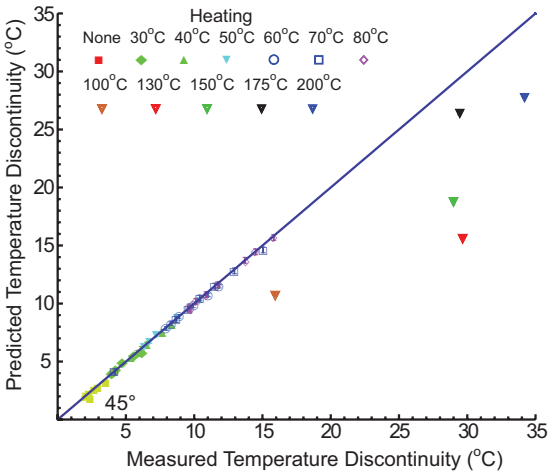

FIG. 7. (Color) The calculated value of the interfacial temperature discontinuity compared with that measured when water evaporated at the rectangular mouth of a PVC funnel. The five experiments for which there is disagreement between the predicted and measured interfacial temperature discontinuities are indicated as those for which the heating element was at a temperature of 100 °C or more. The error bars are shown with the symbol for each experiment, but are not always visible.

ties measured when the vapor-phase heater was set at temperatures up to 80 °C, giving interfacial temperature discontinuities up to 15.69 °C.

These results are in contrast with those obtained when the (constantan) heating element was replaced by a platinum-mica heating element that could be set at temperatures up to 200 °C. All of the results obtained with the PVC funnel listed in Tables III and IV were used to predict the temperature discontinuities shown in Fig. 7. As may be seen there, all of the measurements listed in Table III are consistent with the SRT predictions, but none of those listed in Table IV are consistent. In other words, when the vapor-phase-heating element was set up to 80 °C, and the measured interfacial conditions used with SRT to predict the temperature discontinuities in each of 45 experiments, there was no measured disagreement between the predicted and measured temperature discontinuities, but when the vapor-phase-heating element was set at 100 °C or higher, the predicted temperature discontinuities are in disagreement in each of the five experiments. Thus each of these five experiments is inconsistent with the SRT predictions.

IV. DISCUSSION

When the inconsistency shown in Fig. 7 was found, a series of investigations were performed to determine its source. It was noted that in these five inconsistent experiments, the heating element was set at temperatures of 100 °C or higher; but the operating manual for the pressure gauge used in the experiments (Inficon, SKY Capacitance Diaphragm Gauge, CD0G45, CDG045-H) indicates that the connection of the gauge to the evaporation chamber is limited to temperatures of 90 °C or less. Thus our hypothesis is that in the experiments in which the vapor was heated to

100 °C or higher, the connection of the pressure gauge to the evaporation chamber failed (leaked?) giving a faulty pressure reading. It is essential to know the vapor-phase pressure to predict the temperature discontinuity.

However, there is no reason to assume the interfacial temperature discontinuity reported by [2] is invalid. Thus during steady-state water evaporation experiments, interfacial temperature discontinuities of up to 27.82 °C have been observed along with the corresponding evaporation fluxes. However, the vapor-phase pressure that would exist when the vapor-phase-heating element was set at 100 °C or higher has not been experimentally established. Although it is unusual, this is one case in which theory indicates there was something wrong with the experiments. Normally, it is the other way around.

The results shown in Figs. 4–7 indicate that SRT can be used to predict the measured temperature discontinuities. The interfacial temperatures were measured with microthermocouples. They cannot be placed exactly at the interface because of their finite size, but in some experiments the bead center in the vapor was placed approximately one mean-free path above the interface and in none of the experiments was it more than six mean-free paths away.

In the liquid phase, the bead was within the uniform temperature layer, at least for the experiments described in Table II. Even though the vapor phase was heated electrically, when the thermocouple was within the liquid phase, the thermocouple would be expected to have registered the temperature of the liquid at the position of the bead. In other words, electrical heating of the vapor would not have induced an error in the liquid-phase thermocouple reading. Our procedure for calculating the interfacial-vapor temperature may be viewed as a method of investigating the validity of the vapor-temperature measurement. We take it as known and calculate the temperature in the liquid. If there was a significant error in the measured value of T_I^V, it would be expected to appear when the value of T_I^L was calculated (see Fig. 3) and compared with the measured value that is taken as reliable. The agreement seen in Figs. 4–6 indicates the measured value of T_I^V is also reliable. Also, there is no correlation between the position (number of mean-free paths from the interface) where T_I^V was measured and the calculated value of the temperature discontinuity. In each experiment, except those listed in Table IV, the calculated temperature discontinuity was within the error bars of that measured.

Statistical rate theory was considered as a method for predicting the temperature discontinuities in [1], but their procedure was to linearize the SRT equations. Their linearization was erroneous (see below), and reduced the SRT equations to a triviality. They then concluded "… the expression from [the] SRT treatment do [*sic*] not describe the present steady-state evaporation experimental data." As indicated in previous sections, there is no need to linearize the SRT equations in order to predict the temperature discontinuities, and the nonlinear SRT equations can be used to predict temperature discontinuities that are in agreement with the measurements of [1,2], except for the experiments listed in Table IV in which the vapor-phase pressure was apparently incorrectly recorded.

A consideration of the magnitude of the terms in the SRT expression for the evaporation flux gives insight into the evaporation process at the molecular level. The change in entropy given in Eq. (13) can be written as a sum of two terms. One, $\Delta s_{ct}/k_b$, represents the continuum effects and the value of the other, $\Delta s_{pn}/k_b$, is determined by the interfacial temperatures and the molecular phonons.

TABLE V. Comparison of the continuum and phonon terms in the SRT expression for the entropy change during evaporation. The experiments considered are EA1 of Table I, EO7 of Table II, and Eh45 of Table III.

Expt.:	$10^3\left(\frac{\Delta s_{ct}}{k_b}\right)$	$10^3\left(\frac{\Delta s_{pn}}{k_b}\right)$	$10^3\left(\frac{\Delta s_{LV}}{k_b}\right)$
EA1	3.12	−0.969	2.15
EO7	2.69	−0.182	2.51
Eh45	8.57	−7.04	1.52

The continuum term is given by

$$\frac{\Delta s_{ct}}{k_b} = \left(\frac{v_f}{k_b T_I^L}\right)[P_I^V - P_s(T_I^L)] + \ln\left(\frac{P_s(T_I^L)}{P_I^V}\right) + \left(\frac{v_f \gamma^{LV}}{k_b T_I^L}\right)(C_1 + C_2). \tag{19}$$

Note that the value of $\Delta s_{ct}/k_b$ is determined by the value of P_I^V, T_I^L, C_1+C_2, and the fluid properties, v_f, γ^{LV}, P_s, evaluated at T_I^L. Thus its value does not involve the temperature discontinuity nor the molecular phonons. The values of $\Delta s_{ct}/k_b$ for each of three experiments are listed in Table V.

The phonon dependent term is given by

$$\frac{\Delta s_{pn}}{k_b} = 4\left(1 - \frac{T_I^V}{T_I^L}\right) + \ln\left[\left(\frac{T_I^V}{T_I^L}\right)^4 \left(\frac{q_{vib}(T_I^V)}{q_{vib}(T_I^L)}\right)\right] + \left(\frac{1}{T_I^V} - \frac{1}{T_I^L}\right)\sum_{l=1}^{3}\left(\frac{\hbar\omega_l}{2k_b} + \frac{\hbar\omega_l}{k_b \exp\left(\frac{\hbar\omega_l}{k_b T_I^V}\right) - 1}\right). \tag{20}$$

It does not involve any continuum properties, save the liquid and vapor interfacial temperatures. Its values are also listed in Table V. Note that the phonon term is negative, but recall that $\Delta s_{LV}/k_b$ is, by definition, $(s_L - s_V)/k_b$; thus the fact that $\Delta s_{pn}/k_b$ is negative indicates the contribution of the internal phonons of the water molecule to the entropy at the temperature of the vapor is greater than that at the temperature of the liquid. We emphasize that for none of the experiments is $\Delta s_{pn}/k_b$ negligible compared to the continuum term. Also, since the continuum term and the phonon term are of different signs, the sum is much smaller in magnitude than either term. It is the sum of the continuum and phonon terms that is used to determine the SRT expression for the evaporation flux.

In the analysis presented in [1], the phonon term was completely neglected and the continuum term was severely approximated. When the phonon term is neglected, Δs_{LV} is replaced by Δs_{ct}. This eliminates any dependence of the j_{ev}

on T_I^V. Thus it is then impossible to predict the temperature discontinuity because in their approximation the flux does not depend on the interfacial-vapor temperature T_I^V.

V. CONCLUSION

It is difficult to imagine, but the results indicate that during steady-state water evaporation, the molecules on one side of the interface can be 15.7 °C colder than those on the other side of the interface. This change in temperature happens over a distance of only a few molecular diameters. This finding is supported by measurements made during steady-state water evaporation experiments (Table I–IV) and the predictions made with SRT (see Figs. 4–6). At temperatures below the triple point of water, SRT has been successfully used to predict the independently measured latent heat and the constant-pressure-specific heat from measurements made during both evaporation and condensation [18]. The consistency of the predicted temperature discontinuities with those measured supports the existence of the large temperature discontinuities reported in [1,2]. Also, the agreement between the predictions and the measurements suggests that the thermocouple measurements of the interfacial temperatures in which the center of a thermocouple bead that has a diameter of less than 50 μm and has its center located approximately 35 μm above or below the interface give sufficiently accurate interfacial temperatures to use in the SRT analysis.

The larger the entropy change that results from a molecule going from the liquid to the vapor phase, the larger the evaporation flux, according to SRT. This entropy change can be expressed as a sum of Δs_{ct} and Δs_{pn}. The former results from continuum effects [see Eq. (19)] and the interfacial-liquid temperature and acts as the driving force for evaporation. The latter depends on the phonons of the water molecule and the interfacial temperatures [see Eq. (20)] and is negative. Thus Δs_{pn} acts to inhibit the evaporation flux. The term Δs_{pn} involves the internal (quantum mechanical) states of the water molecule and the temperature discontinuity. Its inclusion is essential to the SRT prediction of the temperature discontinuity. If this term is not included, there is no dependence of the evaporation flux on T_I^V, and the flux expression cannot be used to predict the temperature discontinuity [4].

Interestingly, temperature discontinuities of up to 27.72 °C during steady-state water evaporation (see Table IV) have been reported [2]. There is no reason to doubt the validity of the temperature measurements, but their consistency with SRT cannot be established because of uncertainties in the vapor-phase-pressure measurements.

ACKNOWLEDGMENTS

We gratefully acknowledge the support of the Canadian Space Agency, the Natural Sciences and Engineering Research Council of Canada, the European Space Agency, the University of Erlangen-Nürnberg, and FMP Technology GMBH.

[1] V. K. Badam, V. Kumar, F. Durst, and K. Danov, Exp. Therm. Fluid Sci. **32**, 276 (2007).
[2] V. K. Badam, Ph.D. thesis, University of Erlangen-Nuremberg, 2007 (unpublished).
[3] G. Fang and C. A. Ward, Phys. Rev. E **59**, 417 (1999).
[4] C. A. Ward and G. Fang, Phys. Rev. E **59**, 429 (1999).
[5] C. A. Ward and D. Stanga, Phys. Rev. E **64**, 051509 (2001).
[6] S. Popov, A. Melling, F. Durst, and C. A. Ward, Int. J. Heat Mass Transfer **48**, 2299 (2005).
[7] C. A. Ward and F. Duan, Phys. Rev. E **69**, 056308 (2004).
[8] F. Duan and C. A. Ward, Phys. Rev. E **72**, 056302 (2005).
[9] F. Duan, V. K. Badam, F. Durst, and C. A. Ward, Phys. Rev. E **72**, 056303 (2005).
[10] F. Duan and C. A. Ward, Phys. Rev. E **72**, 056304 (2005).
[11] G. T. Barnes and A. I. Feher, J. Colloid Interface Sci. **75**, 584 (1980).
[12] H. K. Cammenga, D. Schreiber, G. T. Barnes, and D. S. Hunter, J. Colloid Interface Sci. **98**, 585 (1984).
[13] X. Xu and J. Luo, Appl. Phys. Lett. **91**, 124102 (2007).
[14] R. Hołyst and M. Litniewski, Phys. Rev. Lett. **100**, 055701 (2008).
[15] C. A. Ward, J. Chem. Phys. **79**, 5605 (1983).
[16] C. A. Ward, R. D. Findlay, and M. Rizk, J. Chem. Phys. **76**, 5599 (1982).
[17] C. A. Ward, J. Non-Equilib. Thermodyn. **27**, 289 (2002).
[18] F. Duan, I. Thompson, and C. A. Ward, J. Phys. Chem. B **112**, 8605 (2008).
[19] R. D. Present, *Kinetic Theory of Gases* (McGraw-Hill, New York, 1958).
[20] G. Herzberg, *Molecular Spectra and Molecular Structure* (Van Nostrand, Princeton, NJ, 1964), Vol. 2, p. 281.
[21] K. Feldkamp, Chem.-Ing.-Tech. **41**, 1181 (1969).
[22] G. S. Kell, J. Chem. Eng. Data **12**, 66 (1967).